Palacký University Olomouc
Faculty of Science

Department of Optics

Spectral measurement and filtering of light sources using fiber gratings

Bachelor's Thesis

Anežka Dostálová

Palacký University Olomouc
Faculty of Science

Department of Optics

Spectral measurement and filtering of light sources using fiber gratings

Bachelor's Thesis

Author: Anežka Dostálová
Study programme: B1701 Physics
Field of study: Optics and Optoelectronics
Form of study: Full-time
Supervisor: RNDr. Miroslav Ježek, Ph.D.

Thesis submitted on: .....

Univerzita Palackého
Přírodovědecká fakulta

Katedra optiky

Měření a modifikace spektra optických zdrojů pomocí vláknových mřížek

Bakalářská práce

Autor: Anežka Dostálová
Studijní program: B1701 Fyzika
Studijní obor: Optika a optoelektronika
Forma studia: Prezenční
Vedoucí: RNDr. Miroslav Ježek, Ph.D.

Práce odevzdána dne: .....

Abstract

Fiber gratings are nowadays widely used in optical communication and for optical spectra modification in various applications. Typically, they are divided to fiber Bragg gratings and long-period fiber gratings, according to the length of their period. In this thesis, the basic theory of fiber gratings is presented, the possibility of inducing long-period fiber gratings mechanically is explored and the process of their fabrication and performed measurements are described. Finally, two methods of optical spectra measurement are compared.

Keywords

`Long-period fiber grating, Fiber Bragg grating, Mode coupling, Transmission spectrum, Spectroscopy, Temperature dependence`

Acknowledgments

I would like to sincerely thank and express my deepest gratitude to my supervisor RNDr. Miroslav Ježek, Ph.D. for the time he devoted to our consultations and to getting me acquainted with the work in the lab, and for all the valuable advice he gave me. I very much thank Mgr. Michal Dudka for milling the long-period fiber gratings and his help with 3D printing. As for the 3D printing, I also thank Mgr. Robert Stárek, Mgr. Martin Paúr and my brother Matěj for their assistance and advice. I would like to thank all the lectors who guided me through my studies for their enthusiasm, helpfulness and knowledge passed on to me. Special thanks go to my family, who have been extremely supportive throughout my whole life.

Anežka Dostálová

Declaration

I hereby declare that I have written this Bachelor's Thesis—and performed all the presented research and experimental tasks—by myself, while being supervised by RNDr. Miroslav Ježek, Ph.D. I also state that every resource used is properly cited. I agree with the Thesis being used for teaching purposes and being made available at the website of the Department of Optics.

Signed in Olomouc on ....

Anežka Dostálová

Contents

Chapter 1

Introduction

Fiber gratings are structures created by periodic refractive index change and play an important role in optical communications and sensing. When optical signal propagates through an optical fiber, the grating periodicity causes the light of the fundamental core mode to couple to either counter-propagating mode or to radiation cladding modes of the fiber, according to the length of the grating period. The coupling occurs at discrete wavelengths and results in loss notches in the transmission spectrum of the source. This can be advantageously used for a wide range of applications.

As briefly mentioned above, fiber gratings can have different period lengths. This leads to a basic division to short-period and long-period fiber gratings. The short-period grating is best known as fiber Bragg grating and was first written into the fiber core in 1978 [1]. Since that, it has been widely used for example in optical sensors. Characterization, fabrication and other applications of Bragg gratings are reviewed in [2]. Long-period fiber gratings were developed later, but their usage is also increasing. They are very versatile in achieving required spectral characteristics as a lot of their parameters may be tuned [3]. They possess low insertion losses and polarization independence, and unlike fiber Bragg gratings, they have no back-reflection [4], which is desirable for instance in the case of gain equalizers. The original method of fabrication of fiber gratings was UV irradiation of the fiber core. It is still a standard procedure, other have been, however, developed later. Fabrication of long-period fiber grating by thermal shock effect of focused high-frequency CO_2 laser pulses was proposed in [4], which made it possible to induce the gratings in ordinary telecommunication fibers, not just in photosensitive fibers as in the case of UV irradiation. A review of long-period fiber gratings written by CO_2 laser can be found in [5]. When the grating period is long enough, there is an opportunity to induce it mechanically [6].

Optical fiber communication has been significantly expanding over the past decades. Substituting metallic cables with optical fibers brings along notable advantages, for example the ability to transmit large amount of data over long distances with very low losses. The distances are nevertheless limited by fiber attenuation. The transmission distance is typically increased by compensating the attenuation by optical amplifiers. The best known and widespread optical amplifier is erbium-doped fiber amplifier (EDFA), because its maximum gain is around the wavelength 1550 nm, which corresponds well to the wavelength

at which the conventional silica fiber manifests the smallest loss. However, EDFA may have non-uniform gain profile and presents amplified spontaneous emission (ASE), which leads to the need for adjusting the gain spectrum to suppress these undesirable effects. In [7], the usage of long-period fiber gratings for this purpose was proposed. Gain equalization and ASE noise reduction are also demonstrated in [4]. Long-period fiber gratings are suitable for this task for their flexibility and thus the possibility to create a transmission spectrum that matches the inverted gain spectrum [7].

Long-period fiber gratings have also been used as mode converters [8, 9], band-rejection filters [10] or for laser beam shaping [11, 12]. The last mentioned is useful for applications that require a uniform intensity laser beam instead of a Gaussian one, and long-period fiber gratings can be employed for this task of beam transformation. The grating will partially couple the fundamental core mode into a cladding mode and interference of these modes will cause the beam to have a uniform intensity distribution in a certain distance from the end of the optical fiber. Authors of [11] declare their device can perform dynamic shaping of the beam from Gaussian to a donut and a top-hat beam back to Gaussian simply by tuning the laser wavelength. Another growing field of long-period fiber gratings application are optical sensors. In long-period fiber gratings, coupling of the fundamental core mode to radiation cladding modes results in wavelength-dependent losses in the transmission spectrum and is highly sensitive to external conditions like temperature, strain or refractive index of the surrounding environment [13]. First experimental results of the sensing properties of UV induced long-period fiber gratings were reported in [13, 14] and reviewed in [15]. It is shown that the temperature sensitivity is more significant than that of a conventional fiber Bragg grating. As for the sensitivity to the refractive index of the surrounding environment, it arises from the fact that the coupling wavelengths depend on the effective indices of the core and cladding modes, and these effective indices are dependent on the external refractive index [16]. Any modification of it thus leads to a change in the phase-matching condition determining the coupling wavelengths. This allows measuring the refractive index of different liquids knowing their concentration or vice versa [17]. The same principle was applied to creation of a biosensor for detection of cancer biomarkers [18], it is hence evident that long-period fiber gratings are of growing importance and are spreading into other scientific fields. Recently, sensing of torsion, refractive index and temperature was demonstrated and improved with a different type of long-period fiber gratings, so called helical LPFG [19].

This thesis focuses on mechanical fabrication and analysis of long-period fiber gratings and on some methods of optical spectra measurement. In the first chapter, fiber gratings are introduced from the general point of view and short-period and long-period gratings are specified. Fabrication procedure, theoretical model and analysis of long-period fiber gratings are all presented in the next chapter. Third chapter deals with the temperature dependence of fiber gratings. Finally, methods of optical spectra measurement, namely using grating spectrometers and Fourier-transform spectroscopy, are taken into consideration in the fourth chapter and the results obtained from both methods are compared and discussed. The results are summarized in the last chapter and possible future extensions are outlined.

Chapter 2

Fiber gratings

Optical fibers are very thin cylindrical waveguides consisting of a core and a cladding. The light is led through the core due to total reflection, which can only occur if the refractive index of the core is slightly higher than the one of the cladding. Fiber gratings are basically diffraction gratings inside of the fiber, typically few centimetres long, and can be obtained by inducing a periodical change of the core refractive index. This can be achieved for example by periodical ultraviolet irradiation of the core or by mechanical stress.

Two types of fiber gratings can be generally distinguished according to the period length. Firstly, in short-period fiber gratings, or so called Bragg gratings, coupling takes place between opposite travelling modes. Secondly, in the long-period fiber gratings coupling occurs between modes that propagate in the same direction [3]. This thesis focuses mainly on mechanically induced long-period gratings, their fabrication and analysis. However, measurements with UV light induced Bragg grating were performed too in order to demonstrate the basic difference.

2.1 The grating equation

When a light wave falls onto a diffraction grating at an incident angle θ_1, it is diffracted into different directions determined by an angle θ_2. This effect is depicted in Fig. 2.1 and described by the grating equation

$$n \sin \theta_2 = n \sin \theta_1 + l \frac{\lambda}{\Lambda}, \tag{2.1}$$

where n is the refractive index of the surroundings, λ is the wavelength of the incident wave, Λ is the grating period, and $l = \pm 1, \pm 2, ...$ is the diffraction order. For fiber gratings, this equation determines the wavelength at which the most efficient coupling between two modes occurs [3].

In waveguides, light can only exist in the form of modes – self-consistent fields, which means the fields' transverse distribution remains constant during the propagation through the waveguide [20]. Mode propagation constant β is the wavenumber component in the direction of light propagation for a given mode. It is the vacuum wavenumber multiplied by effective refractive index,

$$\beta = \frac{2\pi}{\lambda} n_{\text{eff}}. \tag{2.2}$$

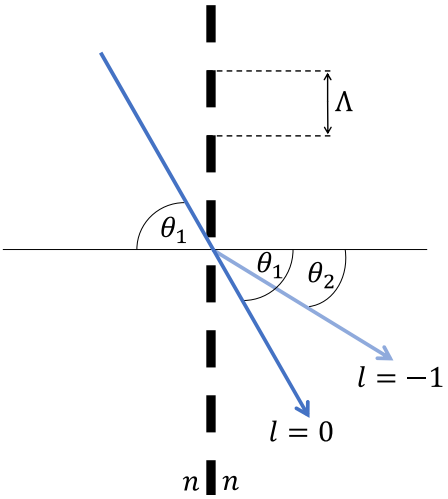

Figure 2.1: Diffraction of light on a grating.

The effective refractive index n_{eff} of the core mode is given by

$$n_{\text{eff}} = n_{\text{co}} \sin\theta, \tag{2.3}$$

where n_{co} is the core refractive index, and depends on the wavelength and on the mode. The modes in the fiber can only exist if the conditions for total reflection are met. As a consequence, the effective index of the guided core modes will always satisfy inequality $n_{\text{cl}} < n_{\text{eff}} < n_{\text{co}}$, the effective index of cladding modes will always satisfy inequality $1 < n_{\text{eff}} < n_{\text{cl}}$.

Using (2.2) and (2.3), the grating equation (2.1) can be rewritten into

$$\beta_2 = \beta_1 + l\frac{2\pi}{\Lambda}. \tag{2.4}$$

This form of the grating equation will lead to equations determining the wavelengths of the most efficient coupling in fiber Bragg grating and long-period fiber grating in the following sections.

2.2 Fiber Bragg grating (FBG)

Short-period fiber gratings, whose period is typically smaller than 1 µm, are called Bragg gratings. The light mode remains the same core mode after having interacted with the Bragg grating, only travels in the opposite direction. It is basically a reflection that occurs for a wavelength satisfying the Bragg condition. That is why FBGs can also be regarded as mirrors or reflectors. Since the mode after the interaction is identical to the fundamental core mode, the effective indices are equal $n_{\text{eff},1} = n_{\text{eff},2}$, but as it travels against the direction of propagation of the fundamental core mode, its propagation constant $\beta_2 < 0$. Using these assumptions and also $l = -1$ as first-order diffraction is dominant, from (2.4) we derive the Bragg condition

$$\lambda_B = 2n_{\text{eff}}\Lambda, \tag{2.5}$$

where Λ is the grating period and n_{eff} is the effective refractive index of the core mode [3]. The effect of a Bragg grating on an input spectrum is shown in Fig. 2.2. The coupling between counter-propagating modes results in a narrow spectral loss in the transmission spectrum at wavelength λ_B. However, as mentioned above, the core mode is reflected from the grating exactly into the opposite direction and remains a core mode, which allows us to detect a reflection of the narrow transmission band. The width of the reflected spectrum is less than 1 nm, usually tenths of a nanometre.

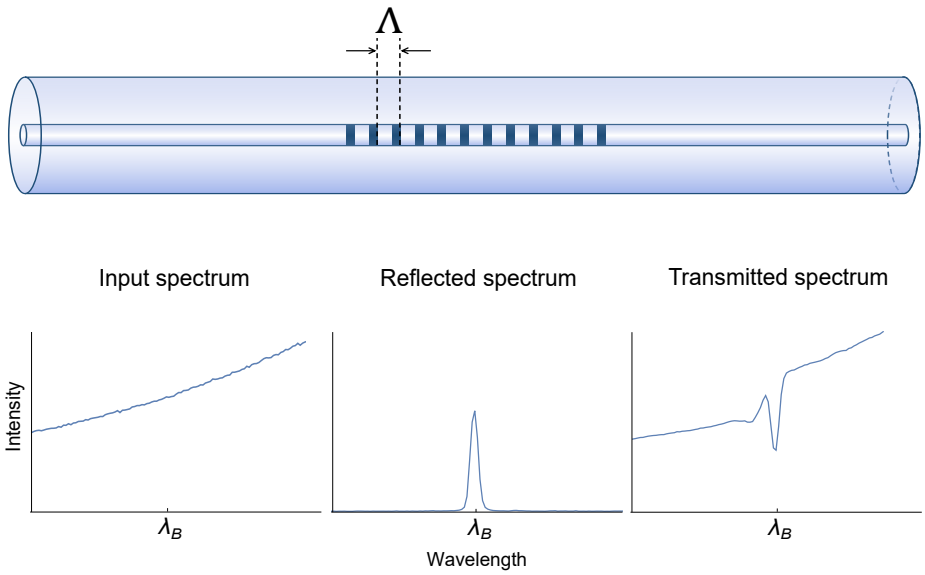

Figure 2.2: Fiber Bragg grating. In the upper part of the figure, a schematic optical fiber with a FBG inscribed in the core can be seen. In the lower part of the figure, the effect of FBG on the input spectrum is demonstrated. The input spectrum around wavelength λ_B, the spectrum of the reflection from the grating at λ_B and the transmitted spectrum are shown, respectively. The spectra were measured by the author of the thesis with a commercially acquired FBG (Safibra) using superluminescent diode as a source and a circulator (discussed in more detail in Sec. 5.1).

Fiber Bragg gratings must be fabricated in a manner that guarantees sufficient resolution regarding the period length. Suitable technique is an exposure of the fiber core to powerful radiation. Two typical methods based on this principle were developed. The permanent periodical change of refractive index can be achieved by simply irradiating discrete spots of the core by CO_2 laser. Either the laser itself is moved by the required period, or the fiber is shifted keeping the laser position fixed. An alternative is so called phase mask technique [21]. An UV light beam impinges on a phase mask which causes its diffraction. The 1st and -1st diffraction order create an interference pattern at the position of the fiber core, if the fiber is placed properly. As a result, the fiber core refractive index is changed where the interference happens to be constructive, with a period corresponding to the one of the pattern.

2.3 Long-period fiber grating (LPFG)

Long-period fiber gratings have a period in the order of hundreds of micrometres. Due to the grating, a fundamental core mode is diffracted into several cladding modes travelling at different angles, but forward just as the core mode. A loss notch is created in the transmission spectrum, similarly to the case of FBG, its width is, however, much larger. The most significant difference between LPFG and FBG is that the light coupled to the cladding modes is radiated away, which makes it impossible to detect any reflection of the filtered spectral band.

The coupling from the core mode to the cladding modes only occurs at particular wavelengths. As there are more cladding modes of different orders m, there are several corresponding wavelengths $\lambda^{(m)}$ at which the modes couple. These coupling wavelengths depend on the grating period and on the induced refractive index change and can be determined from a phase-matching condition derived again from (2.4). In this case, the propagation constant of the cladding modes $\beta_2 > 0$ and the interacting modes are not identical, so neither the effective indices are equal, which leads to a phase-matching condition in the following form

$$\frac{2\pi}{\Lambda} = \frac{2\pi}{\lambda^{(m)}}(n_{\text{effco}} - n_{\text{effcla},m}), \tag{2.6}$$

where Λ is the grating period, n_{effco} is the effective index of the core mode and $n_{\text{effcla},m}$ is the effective index of m-th cladding mode. The left hand side of the phase-matching condition stands for the grating wavenumber, while the right hand side represents wavenumbers of the core mode and m-th cladding mode. Since momentum $p = \hbar k$, the phase-matching condition can be regarded as the law of momentum conservation. As simple as (2.6) may seem, it is actually a highly non-trivial numerical problem. This is due to the fact that both n_{effco} and $n_{\text{effcla},m}$ are wavelength and mode dependent. They also depend on parameters of the specific optical fiber. Numerical solution to this problem will be presented in Sec. 3.2.

As for fabrication of long-period fiber gratings, exposure to powerful radiation can be used similarly to the case of fiber Bragg gratings. However, the period size of hundreds of micrometres is already big enough to offer an interesting possibility of inducing the refractive index change mechanically. This will be discussed in detail in Sec. 3.1 as the mechanical fabrication of LPFGs was one of the main goals of this thesis.

Chapter 3

Analysis of LPFGs

The main focus of this thesis was fabrication of long-period fiber gratings and analysis of their effect on light sources spectra. LPFGs for our purposes were manufactured by 3D printing and milling and it will be described in the first section of this chapter. In the next section, dispersion relations for computation of effective indices will be numerically solved in order to predict the relation between the grating periodicity and the wavelength, at which the coupling between the fundamental core mode and co-propagating cladding modes takes place. The last section contains a description of the performed measurements and discussion of the results.

3.1 Fabrication

There are several ways to produce long-period fiber gratings. In Sec. 2.2, possible techniques of inscription of fiber Bragg gratings were briefly described. The same techniques can be applied when producing long-period fiber gratings, the only difference being the period length (and thus longer shifts of the fiber or the laser in case of irradiating discrete spots of the fiber core, or a different design of the phase mask in case of the phase mask technique). In contrast to the FBG, there rises an interesting opportunity for the LPFG to be induced mechanically, as its typical period is a fraction of a millimetre. This new approach to the fabrication brings along huge advantages – unlike in the case of radiation induced periodical refractive index change, the change induced mechanically is not permanent, which means the fiber can be later used for other purposes or with a grating of a different length and period. Furthermore, the fiber does not have to be photosensitive, which makes LPFGs even more feasible.

For 3D printing of the LPFGs, models were created with the use of software Autodesk Inventor and online program Tinkercad. They were then printed on Original Prusa printer. PLA material was used in all cases. It is the most commonly used material in 3D printing, and it has the best ability to print tiny details, which was convenient for our purposes. However, the structure on the top of the grating must be precise and its details are very close to the printer resolution limit, which made it difficult to obtain a reliably functioning grating. Different printing strategies, for example the position and placement of the grating on the build plate, were examined. Also different profiles of the

upper structure were tested, the best one turned out to be a triangular one. An example of both the model and the printed result is shown in Fig. 3.1.

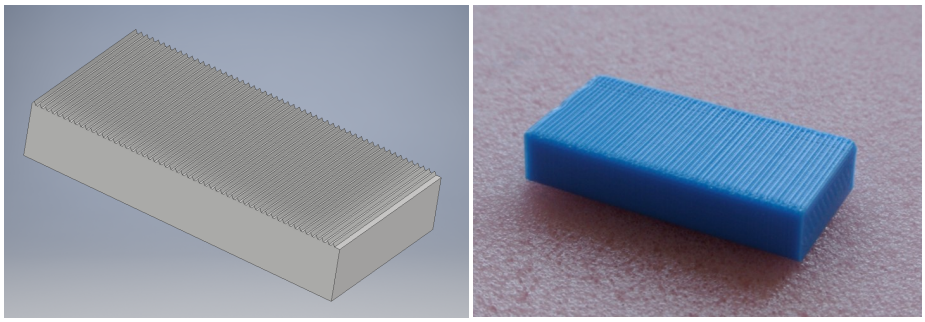

Figure 3.1: A model of a long-period fiber grating with a period 550 µm created in Autodesk Inventor and the printed result.

Milled LPFGs were manufactured by M. Dudka out of a material called Cuprextite, which is an epoxy resin clad with copper on one side. The problem with the milling was again the small and precise structure on the top of the gratings, it was thus not possible to guarantee the production of precisely the same grating sometime later. Consequently, each milled grating had a slightly different side profile of the crucial upper structure. An example of a milled grating is shown in Fig. 3.2.

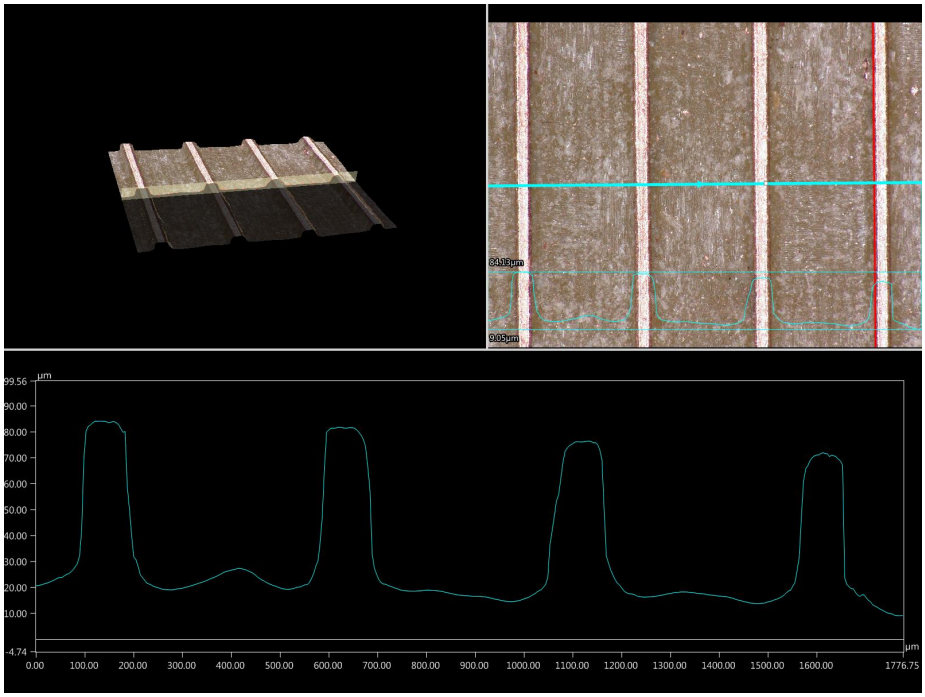

Figure 3.2: A profile of a milled grating with a period approximately 500 µm.

Gratings with periods in range from 300 µm to 600 µm were produced in general. However, the region of periods covered by both techniques was from 450 µm to 550 µm. This is mainly due to the fact that the shortest possible period to obtain a functional grating managed by 3D printing was 450 µm. The effect on the spectral transmittance was examined for all the gratings in the first step; only the ones providing some reproducible results were used in further measurements.

3.2 Theoretical model

To determine the wavelengths at which a LPFG of a given period causes coupling of the fundamental core mode to the forward-propagating cladding modes, the phase-matching condition (2.6) must be solved. It was already mentioned that it is a simple equation at the first sight, a highly complicated numerical problem is, however, hidden behind it because of the effective indices of the core and cladding modes.

The effective indices may be numerically obtained from dispersion equations presented by Erdogan [22]. A few errors appeared in the original article, they were corrected according to the errata [23] and are stated here in the form used in the numerical solution. The dispersion relation, from which the effective index of the fundamental core mode can be computed, is given by

$$V\sqrt{1-b}\frac{J_1(V\sqrt{1-b})}{J_0(V\sqrt{1-b})} = V\sqrt{b}\frac{K_1(V\sqrt{b})}{K_0(V\sqrt{b})}, \tag{3.1}$$

where $V = (2\pi/\lambda)\mathrm{NA}a_{core}$ is the normalized frequency, $b = (n_{\mathrm{eff}}^2 - n_2^2)/(n_1^2 - n_2^2)$ is the normalized propagation constant, J_m is a Bessel function of the first kind, K_m is a modified Bessel function of the second kind, NA is the numerical aperture, n_1 and n_2 are the core and cladding refractive indices, respectively. The dispersion relation for cladding modes is much more complicated and it is of the form

$$\xi_0 = \xi_0', \tag{3.2}$$

where

$$\xi_0 = \frac{1}{\sigma_2}\frac{u_2\left(JK + \frac{\sigma_1\sigma_2 u_{21}u_{32}}{n_2^2 a_1 a_2}\right)p_m(a_2) - Kq_m(a_2) + Jr_m(a_2) - \frac{1}{u_2}s_m(a_2)}{-u_2\left(\frac{u_{32}}{n_2^2 a_2}J - \frac{u_{21}}{n_1^2 a_1}K\right)p_m(a_2) + \frac{u_{32}}{n_1^2}q_m(a_2) + \frac{u_{21}}{n_1^2 a_1}r_m(a_2)}, \tag{3.3}$$

$$\xi_0' = \sigma_1\frac{u_2\left(\frac{u_{32}}{a_2}J - \frac{n_3^2 u_{21}}{n_2^2 a_1}K\right)p_m(a_2) - \frac{u_{32}}{a_2}q_m(a_2) - \frac{u_{21}}{a_1}r_m(a_2)}{u_2\left(\frac{n_3^2}{n_2^2}JK + \frac{\sigma_1\sigma_2 u_{21}u_{32}}{n_1^2 a_1 a_2}\right)p_m(a_2) - \frac{n_3^2}{n_1^2}Kq_m(a_2) + Jr_m(a_2) - \frac{n_2^2}{n_1^2 u_2}s_m(a_2)}. \tag{3.4}$$

The parameters used in (3.3) and (3.4) are defined in the following manner:

$$\sigma_1 = i \cdot m \cdot n_{\mathrm{effcla},m}/Z_0, \tag{3.5}$$

$$\sigma_2 = i \cdot m \cdot n_{\mathrm{effcla},m} Z_0, \tag{3.6}$$

$$u_1 = \frac{2\pi}{\lambda}\sqrt{n_1^2 - n_{\mathrm{effcla},m}^2}, \tag{3.7}$$

$$u_2 = \frac{2\pi}{\lambda}\sqrt{n_2^2 - n_{\mathrm{effcla},m}^2}, \tag{3.8}$$

$$w_3 = \frac{2\pi}{\lambda}\sqrt{n_{\mathrm{effcla},m}^2 - n_3^2}, \tag{3.9}$$

$$u_{21} = \frac{1}{u_2^2} - \frac{1}{u_1^2}, \tag{3.10}$$

$$u_{32} = \frac{1}{w_3^2} + \frac{1}{u_2^2}, \tag{3.11}$$

$$J = \frac{1}{2}\frac{J_{m-1}(u_1 a_1) + J_{m+1}(u_1 a_1)}{u_1 J_m(u_1 a_1)}, \tag{3.12}$$

$$K = \frac{1}{2}\frac{K_{m-1}(w_3 a_2) + K_{m+1}(w_3 a_2)}{w_3 K_m(w_3 a_2)}, \tag{3.13}$$

$$p_m(r) = J_m(u_2 r)Y_m(u_2 a_1) - J_m(u_2 a_1)Y_m(u_2 r), \tag{3.14}$$

$$q_m(r) = J_m(u_2 r)Y'_m(u_2 a_1) - J'_m(u_2 a_1)Y_m(u_2 r), \tag{3.15}$$

$$r_m(r) = J'_m(u_2 r)Y_m(u_2 a_1) - J_m(u_2 a_1)Y'_m(u_2 r), \tag{3.16}$$

$$s_m(r) = J'_m(u_2 r)Y'_m(u_2 a_1) - J'_m(u_2 a_1)Y'_m(u_2 r). \tag{3.17}$$

For purchased optical fibers, the exact values of the core and cladding radii and of the refractive indices n_1 and n_2 are typically not known. The refractive indices may be computed using the Sellmeier equation containing six parameters, which are material dependent and are obtained experimentally. These Sellmeier coefficients are known for fused silica, but a problem rises in case of the fiber cores as they are doped with some other substances in order to distinguish the refractive indices of the core and cladding. The equation can be solved with the usage of some standardized values, though.

In the numerical solution, typical parameters of a standard telecommunication optical fiber were considered, which means the core radius $a_1 = 4.1$ µm and the radius of the cladding $a_2 = 62.5$ µm, numerical aperture was NA $= 0.12$. Refractive index of the cladding n_2 was taken into account as a wavelength dependent, using Sellmeier formula with specific coefficients known for fused silica [20]

$$n_2^2(\lambda) = 1 + \frac{0.6961663\lambda^2}{\lambda^2 - 0.0684043^2} + \frac{0.4079426\lambda^2}{\lambda^2 - 0.1162414^2} + \frac{0.8974794\lambda^2}{\lambda^2 - 9.896161^2}. \tag{3.18}$$

Core refractive index was then obtained from the relation between numerical aperture and the refractive indices

$$\mathrm{NA} = \sqrt{n_1^2 - n_2^2}. \tag{3.19}$$

External refractive index n_3 was set to 1 for a stripped fiber. Equations (3.1) and (3.2) with the above specified parameters' values were numerically solved in Wolfram Mathematica and effective indices were obtained as a function of wavelength as a result. The acquired curves are plotted in Fig. 3.3.

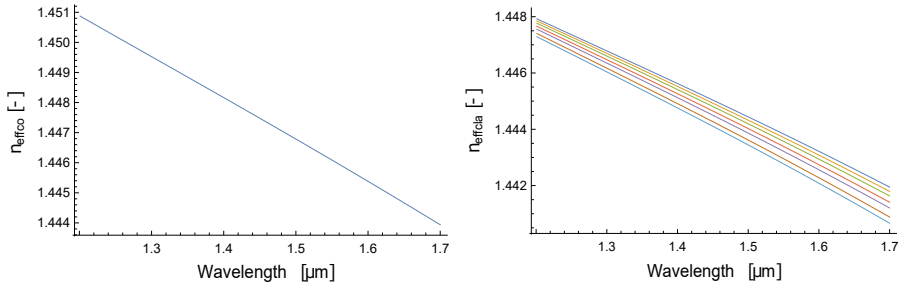

(a) (b)

Figure 3.3: The computed (a) effective index of a fundamental core mode and (b) effective indices of cladding modes.

The differences of the core effective refractive index and cladding refractive indices Δn_{eff} are then used for the computation of grating periodicities for which the coupling between the fundamental core mode and cladding modes occurs. Equation (2.6) can be rewritten into

$$\Lambda = \frac{\lambda}{\Delta n_{\text{eff}}}. \tag{3.20}$$

By substituting the computed values of Δn_{eff} and the values of respective wavelengths into it, dependence of the coupling wavelength on the grating period is obtained, see Fig. 3.4.

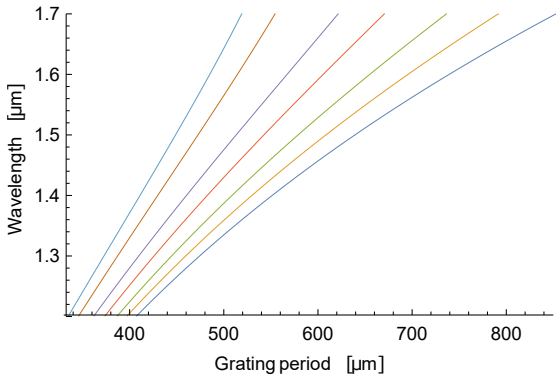

Figure 3.4: Numerically obtained dependence of the coupling wavelength on the length of the grating period.

3.3 LPFGs characterization

Once the long-period fiber gratings were produced, the next step were spectral measurements in order to experimentally determine the effect of these gratings. The periodic change of the refractive index of the fiber core induced by pressing the grating against the fiber causes coupling between the fundamental core mode and cladding modes at particular wavelengths, which are dependent on the

grating period. A simplified schema of the typical experimental setup is shown in Fig. 3.5, as well as a photo of the mechanical construction whose purpose will be described shortly. In the first instance, a halogen lamp was used as the light source for its broad spectrum, which made it possible to see the behaviour of the gratings in a wide range of wavelengths. As much optical signal from the lamp as possible was coupled to a 780-HP optical fiber using fiber collimator (60FC-0-M11-18 from Schäfter+Kirchhoff) and an auxiliary concave mirror in order to increase the amount of signal entering the fiber. Another optical fiber of the same type was connected to the first fiber, it was, however, stripped of the primary buffer on a certain part. This unprotected part was positioned under a mechanical construction with a micrometric screw, which served as a device for applying pressure on the grating placed between the construction and the fiber. The applied pressure on the grating from above caused a periodical deformation of the fiber and thus a periodical change of the core refractive index. The signal was led through another fiber into a spectrometer and the spectrum was processed on a computer.

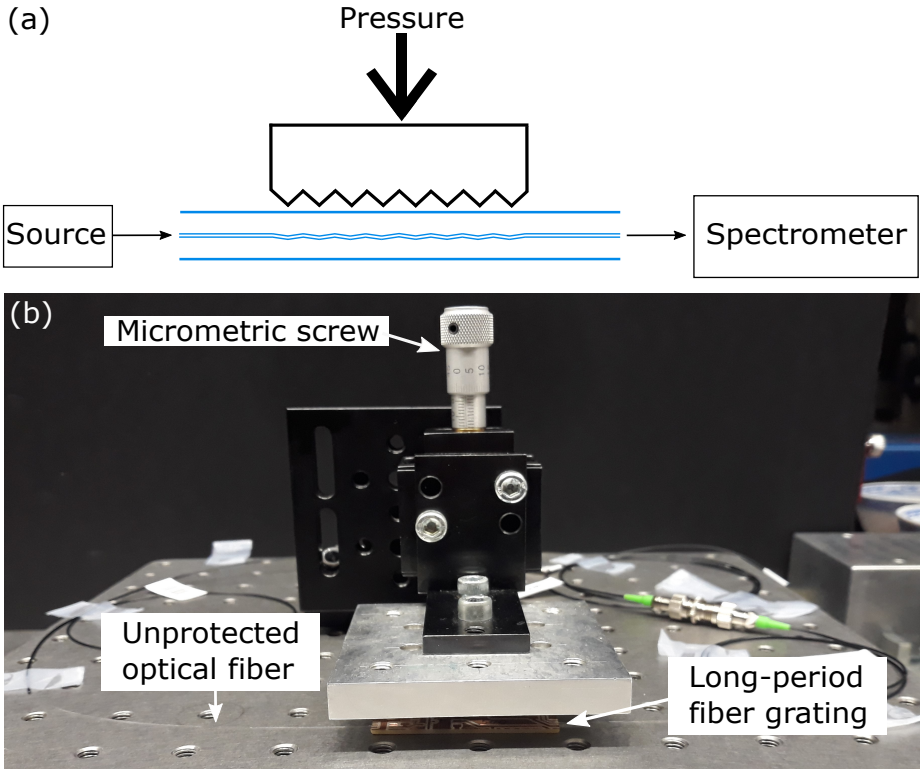

Figure 3.5: (a) A simplified schema of the setup used for spectral measurements with long-period fiber gratings and (b) a photo of the mechanical construction used for applying pressure on the grating and thus on the optical fiber, causing a periodical change in the core refractive index.

Initially, Ocean Optics HR2000+ Spectrometer which covers the whole visible region of the electromagnetic spectrum was employed for the analysis of the output spectra. All the milled and 3D printed long-period fiber gratings

were placed one after another between the mechanical construction and the optical fiber and pressed against the fiber by adjusting the micrometric screw. Usual procedure was such that the background noise spectrum was stored before applying any pressure, then the halogen lamp was switched on and after few minutes, when the power was stabilized, its inherent spectrum was stored as a reference spectrum. The quantity of our interest was mainly spectral transmittance. It is obtained as a ratio of the measured spectrum to the reference spectrum, the noise spectrum being subtracted from both. Some of the gratings did not present any interesting influence on the spectral transmittance, which is due to their poor-quality upper structure. However, in most of the cases the grating caused one or more loss notches at different wavelengths. The notches emerged at the same position for both milled and 3D printed gratings of the same period. An example of a loss notch in the transmission spectrum of a halogen lamp created by a 3D printed LPFG with a period $\Lambda = 450$ µm, occuring at wavelength $\lambda = 727.9$ nm, is shown in Fig. 3.6. The effect of increasing pressure is also demonstrated. The full width at half maximum (FWHM) of the notch created by pressure p_5 is 13 nm. A major issue is to somehow quantify the applied pressure. The only controllable quantity is the exact position of the micrometric screw. When adjusted carefully, it is possible to reach approximately the same modulation for the same adjustment of the screw. Even though this is not facile to achieve because of the necessary precision, it is always possible to obtain the same depth of modulation by adjusting the screw till the desired value is reached. The increasing pressure in the figure is denoted by p_i and the screw was shifted equidistantly between them.

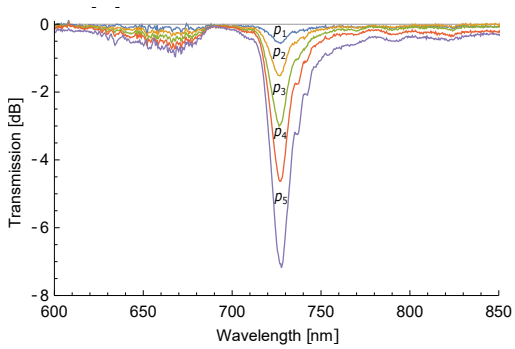

Figure 3.6: An effect of a 3D printed grating ($\Lambda = 450$ µm) and its modification with increasing pressure.

The loss notches in the transmission spectrum created by 3D printed and milled long-period fiber gratings with period $\Lambda = 500$ µm are compared in Fig. 3.7a. To demonstrate the reproducibility of the effect of the produced LPFGs, Fig. 3.7b shows a comparison of the loss notches caused by a 3D printed grating with period $\Lambda = 550$ µm in two separate measurements, which took place with a time delay and the grating was removed in the meantime.

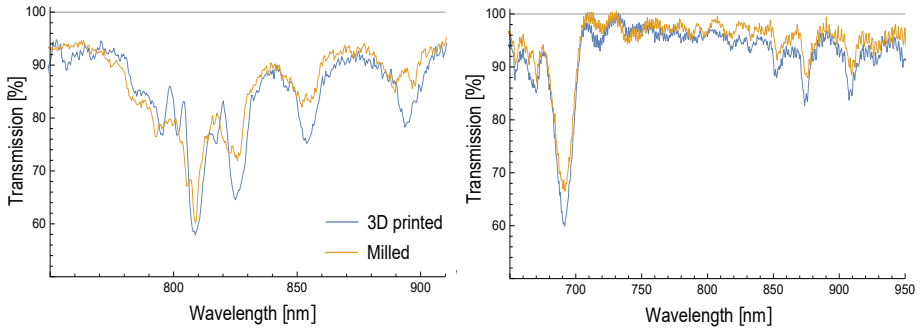

(a) (b)

Figure 3.7: Comparison of (a) the effect of 3D printed and milled grating with the same period $\Lambda = 500$ µm on the source transmission spectrum and (b) the effect on the transmission spectrum obtained in two separate measurements with the same 3D printed grating with period $\Lambda = 550$ µm.

The behaviour of the transmission spectrum under the influence of LPGFs was also studied at telecommunication wavelengths. Those are wavelengths approximately in range 1100–1700 nm and it is the region where optical communications take place. Fiber gratings are commonly studied and used in this wavelength range and have been rarely examined in near infrared region. The main principle of the setup was preserved, the individual components had to be nevertheless replaced by ones suitable for the new range of wavelengths. Optical fibers 780-HP were substituted by SMF-28e$^+$ single-mode fibers and Ocean Optics NIRQuest512 Spectrometer was used. The halogen lamp remained the light source, because its spectrum is sufficiently wide. Only the acquisition time had to be prolonged to 1 s. While performing the measurements, it turned out that the transmission loss notches reach much lower percentage even at smaller applied pressure than in the visible region of wavelengths. A loss notch caused by $\Lambda = 475$ µm milled grating and its development with increasing pressure is shown in Fig. 3.8. The coupling in this case occurs at wavelength $\lambda = 1249.9$ nm and the FWHM of the deepest notch is 27 nm.

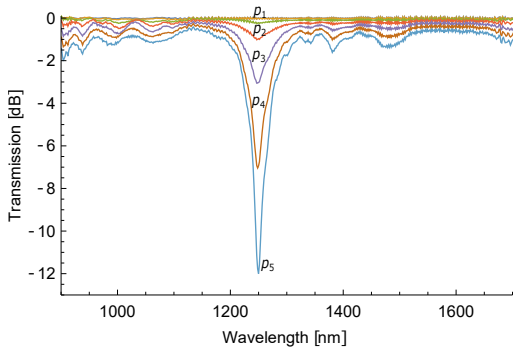

Figure 3.8: An effect of a milled grating ($\Lambda = 475$ µm) and its modification with increasing pressure.

The range of the fabricated gratings periodicities was larger in the case of milled LPFGs, that is why they were chosen for a further analysis of their effect on the transmittance spectrum. Experimentally obtained dependence of the coupling wavelength, i.e. the wavelength where the loss notches arise, on the grating period is plotted in Fig. 3.9.

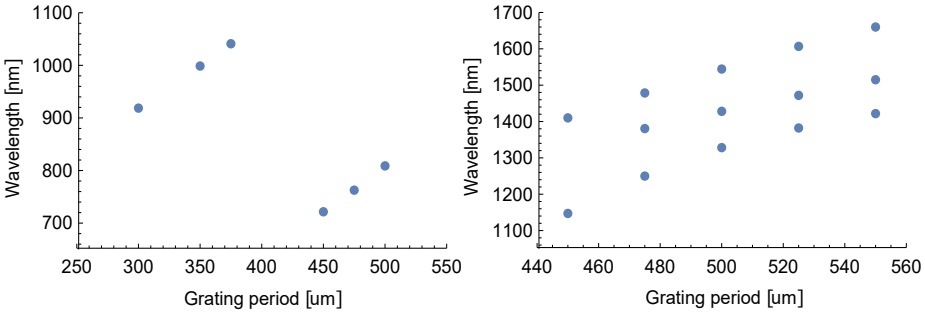

(a) (b)

Figure 3.9: Coupling wavelength versus grating period (a) in the visible and beginning of near infrared region and (b) at telecommunication wavelengths.

If we compare the measured data shown in Fig. 3.9b with the curves computed from the analytical model, which are in the same wavelength region and are plotted in Fig. 3.4, the model fits the data surprisingly well, see Fig. 3.10, considering all the approximations made and the uncertainty of the fiber parameters. The theoretical modelling is highly sensitive to all technical parameters of the specific optical fiber. The computation of the grating period versus coupling wavelength dependence is extremely sensitive to the precision of determination of the effective indices difference Δn_{eff}, whose values are typically of the order of 10^{-4}. This is most likely the main cause of the imperfect correspondence between the data points and the model, as the exact values of the parameters were not known for the used fiber, not even the doping substances of the fiber core which further influence the exact value of its refractive index.

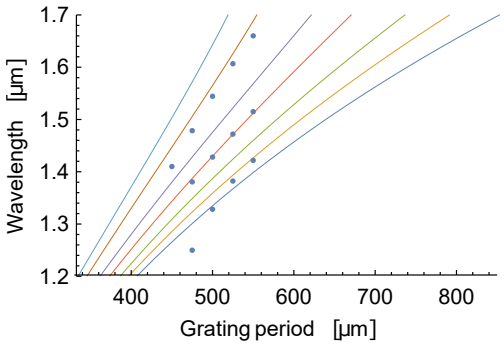

Figure 3.10: Experimentally obtained data points in comparison with the theoretically computed curves. The model fits the data surprisingly well, taking into account the extreme sensitivity of all the fiber parameters, whose exact values were not known.

Even though there are some deviations between the experimental data points and the computed model, in Fig. 3.9 we can clearly observe individual branches corresponding to particular modes and the tendency of the dependence akin to the one of the model, i.e. the coupling wavelength increases with growing length of the grating period for each mode.

To achieve more accurate agreement between the model and the data, it is essential to know the exact Sellmeier formula for the fiber core, including the doping substances, and all the other parameters. With a precise knowledge of the specific fiber parameters, it would also be possible to perform a detailed numerical solution to the Maxwell equations of the field in the fiber, which would even eliminate any approximations made while deriving the analytical formulas stated in Sec. 3.2 and provide very accurate results.

Chapter 4

Temperature dependence

One of the significant applications of both fiber Bragg gratings and long-period fiber gratings is sensing. That is because the coupling between modes is dependent on the effective indices of the core and cladding modes, which are both dependent on the external conditions. One of the conditions influencing the position of the created loss notches in the transmission spectrum is temperature. In this chapter, measurement of the coupling wavelength temperature dependence of the mechanically induced LPFG and commercially obtained UV induced FBG is described.

4.1 LPFG

The experimental setup presented in Sec. 3.3 was modified by adding Peltier element under the part of the optical fiber with no secondary buffer so that the long-period fiber grating lied on it when pressed against the fiber. The adjusted schema is shown in Fig. 4.1. When electric current is passing through a circuit made of two different conductors, then one of the junctions starts to heat up while the other starts to cool down. This phenomenon is called Peltier effect and it is complementary to Seebeck effect, whose essence is a presence of voltage between two different conductors or semiconductors if there exists a temperature gradient between them. We used the Peltier effect to set a required temperature by connecting the Peltier element to a temperature controller (Thorlabs, TED4015). Before the measurement, it was checked that the PID parameters (proportional, integral and derivative) were properly set, so that the temperature remained stable after having been set to the required value and its fluctuations were minimized.

For temperature sensing with long-period fiber gratings, it is crucial that the coupling wavelength shifts with the temperature by a known value. And typically, this is exactly what happens in case of in-fiber UV induced gratings. However, with our mechanically induced long-period fiber gratings, we were not able to prove any direct temperature dependence of the coupling wavelength. Four different milled and two 3D printed gratings were measured. The temperature of the Peltier element was changed from 22 °C to 62 °C. For some of the gratings, the coupling wavelength remained exactly the same during the whole process of increasing the temperature. For other ones, the coupling wavelength

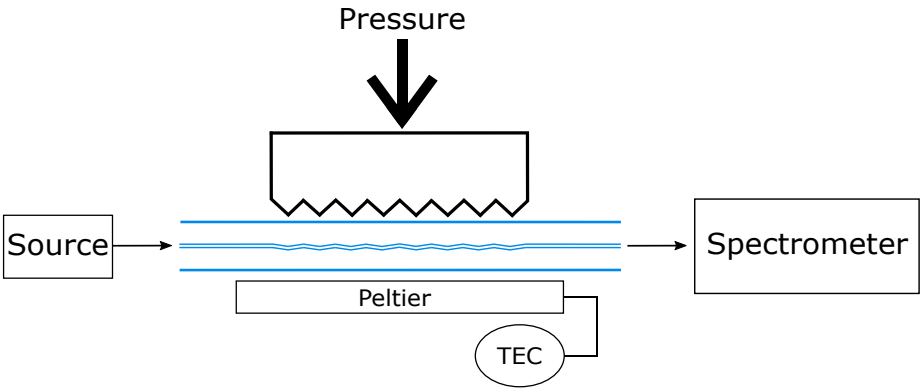

Figure 4.1: A simplified schema of the experimental setup for measuring the temperature dependence of long-period fiber gratings.

shifted to longer wavelengths with higher temperatures, the problem, however, is the fact that after returning to the initial value of the temperature, the coupling wavelength did not shift back to its original position. In a lot of cases, the resultant transmission spectrum was even damaged in comparison to the original one. What changed in all the measurements with no exception was the depth of the created loss notch. That is most likely due to the thermal expansion of the Peltier element, which resulted in different pressure between the optical fiber and the grating lying on it.

This makes the mechanically induced LPFGs inapplicable in temperature sensing. The absence of the dependence may, however, be beneficial in other applications. In [24], for example, the temperature dependence of UV induced LPFGs was required to be eliminated in order to achieve temperature-insensitive sensors of chemical concentration and refractive index. A number of approaches for the temperature sensitivity to be diminished were developed, such as doping a host fiber with a special substance which has the temperature dependence of its refractive index with the opposite sign so compensation takes place [25] or polymer coating of the fiber [26]. Authors of [24] present another method based on bending effect annulling the temperature one. To my knowledge, in most cases the temperature dependence was measured for UV induced LPFGs. Mechanically induced LPFGs were taken into consideration in [6], the authors' procedure was nevertheless different. They immersed the fiber with the grating into water and were changing the temperature of the water. The effective indices are, however, dependent also on the refractive index of the surroundings and the refractive index of the water varies with temperature, that is why it cannot be appropriately compared to our method, where the fiber as well as the grating remained surrounded by air throughout the whole measuring procedure.

In respect to the above mentioned, the measuring procedure was slightly modified by injecting a water drop around the unprotected part of the optical fiber lying on the Peltier element so that there was not air but water between the element and the long-period fiber grating pressed against it. The following steps were identical to the original procedure. The fiber in this case was, however, stripped, which proved to be a better choice as the transmission spectrum was more stable with the changing temperature and returned to its original position

after getting back to the initial temperature. Depth development of the loss notches appeared similarly. Nonetheless, conclusive temperature dependence of the coupling wavelength was not found even with this kind of measuring process. As a consequence, this way of producing long-period fiber gratings may be profitable for creating sensors which are required to be temperature independent.

4.2 FBG

Fiber Bragg gratings may also serve as temperature sensors. Another thing is that when FBGs are fabricated, an arbitrary period can be achieved. The whole process, however, has its limits, and it is thus not possible to reach the central wavelength λ_B with an arbitrary accuracy. Such a fine tuning is usually accomplished by adjusting the temperature, because the attainable range of temperatures is large and the temperature stabilization is very accurate (0.001 K easily). This is a standard tuning method and narrowband frequency tunable filters are typically Bragg gratings. The dependence was verified for commercially available Bragg grating (Safibra) with specified central wavelength 809.97 nm. The temperature of the Peltier element was changed from 22 °C to 50 °C with a step of 1 °C and at each temperature, the reflected spectrum was acquired. The dependence of the wavelength λ_B at which the reflection appears on the set temperature is plotted in Fig. 4.2. The dependence is apparently linear and was fitted with a line $\lambda_B = 809.7643 + 0.0076t$. The average temperature sensitivity of this particular FBG is thus 7.6 pm/K. Knowledge of this value will be useful in future experiments performed in our lab.

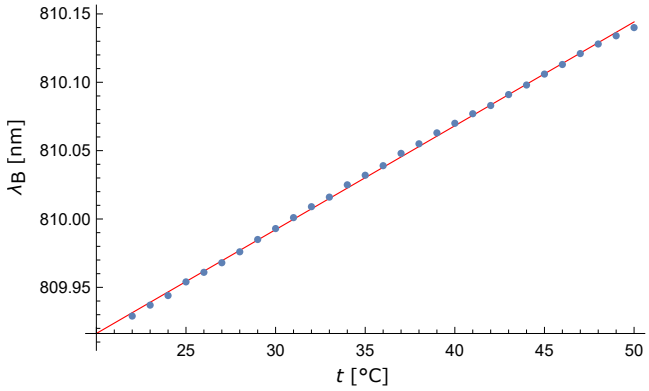

Figure 4.2: Plot of the measured temperature dependence of the central wavelength λ_B of fiber Bragg grating (blue dots) and a fitted curve (red line).

Chapter 5

Methods of optical spectra measurement

5.1 Grating spectrometers

An optical spectrometer is a device capable of determining the intensity of a light source as a function of wavelength. Its most important part is a diffraction element, which distinguishes the wavelengths [27]. A simple schema of a grating spectrometer is shown and described in Fig. 5.1.

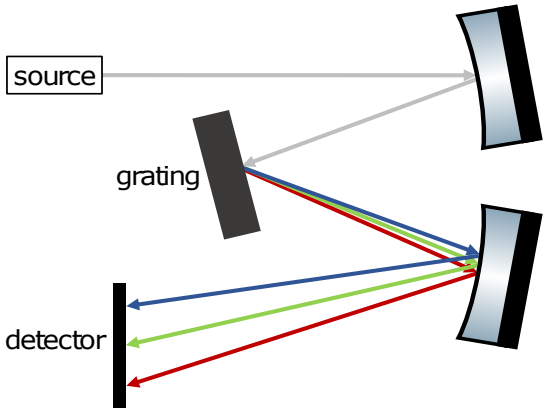

Figure 5.1: A schema of a grating spectrometer. Collimated light emitted from the source falls onto the first mirror. There is a diffraction grating placed in the direction of the reflected light. The grating causes the light to diffract, individual wavelengths are separated. The diffracted light is reflected from the second mirror and falls onto a detector, which registers the intensity distribution in dependence on wavelength. The observed resulting curve is called the spectrum of the light source. The resolution is determined by the number of the grating slits per the area of the grating covered by the incident beam.

For the first spectra measurement, the Ocean Optics HR2000+ Spectrometer was used. Before any measurement took place, the spectrometer was calibrated using a mercury-argon calibration light source (Ocean Optics,

CAL-2000). Since the wavelength 810 nm is of our interest, the calibration focused on the closest spectral line, which is a spectral line of argon on wavelength 811.53 nm. Analysis of the measured spectrum showed that this line appears at wavelength 811.4 nm. Thus, the shift in wavelength the spectrometer makes is 0.13 nm to the left.

Then spectra of different widths were measured. In all cases, from here till the end of this chapter, all the spectra are assumed to be Gaussian, which is an approximation especially in the case of the polarization filter, but it is crucial for the used approach of determining the spectral widths and for the formulas used in Sec. 5.2. The uncertainty of the results obtained by the spectrometer was based on full width at half maximum of the spectrometer response function specified by the manufacturer. The first light source was a superluminescent diode with central wavelength $\lambda = 810$ nm. Spectral data were fitted with a Gaussian curve and its width at $1/e$ of the maximum value was determined to be (29.578 ± 0.021) nm.

In the next measurement, a 3 nm polarization filter designed for the central wavelength of the source (810.57 nm) was added into the setup. 3 nm filter means that the spectral width of the beam transmitted through the filter should be 3 nm. However, this width is usually specified at half maximum, here the width was determined again at $1/e$ of the maximum, which means the obtained value should be greater than 3 nm by a factor of $\sqrt{2 \ln 2}$. The same analysis of data as in the previous case provided a value of (3.456 ± 0.021) nm for the width of the transmitted spectrum at $1/e$ of the maximum.

The narrowest measured spectrum was the reflection from fiber Bragg grating (Safibra), which was added into the setup after removing the 3 nm filter. However, the setup had to be adjusted, because if the fiber containing the Bragg grating was simply connected between the superluminescent diode and the spectrometer, the transmission spectrum would be seen at the output. The desired reflection propagates in the opposite direction, so in order to detect it, an optical circulator must have been added into the setup. The used fiber optic circulator (OZ Optics) has three ports, one of which (T – transmitter) serves as an input and the other two are for transmitted light of the source (1) and light reflected in the output fiber, proceeding in the opposite direction (R – receiver). It allows us to make use of the reflected light, which is exactly what we need in the case of FBG. The adjusted setup was as follows: light from the source was led through an optical fiber connected to the input fiber of the circulator (T). The light further proceeded into the output fiber (1) to which the FBG was connected. The other end of the FBG was covered since we were interested in the reflected spectrum, not in the transmitted one. The reflection from the grating was led to the third port of the circulator (R) and finally, this signal was brought to the spectrometer input fiber. The obtained value of the spectral width was (1.090 ± 0.021) nm.

5.2 Fourier-transform spectroscopy

Spectra of some sources are beyond the spectrometer resolution limit or very close to it, as we could see in the above mentioned reflection from Bragg grating. This is a reason why a more suitable method of spectra measurement is more appropriate in such cases.

The essence of Fourier-transform spectroscopy is the relation between the coherence length of a continuous light source and the width of its spectrum. Coherence length represents the longest possible optical path difference of two waves coming from a single source for an interference to occur. The longer the coherence length, the narrower the spectrum and vice versa.

To observe interference, several conditions must be met. The two interfering waves must be coherent, their frequency must be the same, the amplitudes comparable and their states of polarization must not be orthogonal. The best way to achieve interference practically is to use waves coming from a single light source. The waves meet with a variant phase difference at different points of the screen. It leads to a creation of an interference pattern – bright fringes are formed in places where the waves are in phase, dark fringes, on the other hand, form where the waves meet with an opposite phase.

The contrast between bright and dark fringes is quantified by what is called visibility V. It is a dimensionless number from an interval $\langle 0,\, 1\rangle$ defined as

$$V = \frac{I_{max} - I_{min}}{I_{max} + I_{min}} \tag{5.1}$$

The Fourier-transform spectroscopy will use this quantity as it is comfortably measurable. Visibility versus optical path graph is a Gaussian curve for Gaussian spectra and its relation to the coherence length L of a light source, which is crucial for the measurement, is shown in Fig. 5.2.

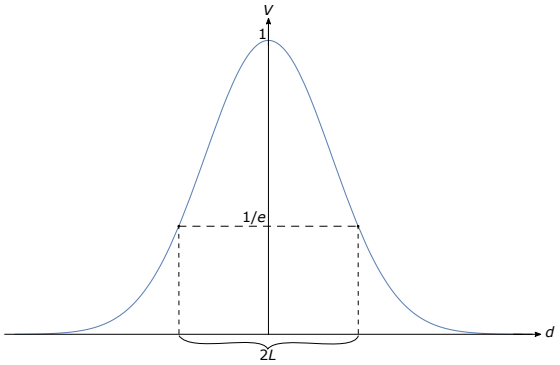

Figure 5.2: A graphical representation of the relation between the visibility versus optical path curve and coherence length of a light source. The distance on horizontal axes between points on the curve where the value of visibility reaches $1/e$ of its maximum value equals two times coherence length.

For the spectrum of measured sources will be assumed to be Gaussian, the coherence length can be obtained from a following formula:

$$L = \sqrt{\frac{2\ln 2}{\pi}}\frac{\lambda^2}{n\Delta\lambda}, \tag{5.2}$$

where λ is the central wavelength of the source and $\Delta\lambda$ is the width of the source emission spectrum at $1/e$ of the maximum value, which is the merit of our interest [28].

A way to obtain two light beams with a particular optical path difference, coming from a single source in order to fulfil requirements for interference, is to build Michelson's interferometer. The basic setup used in the experiment is depicted in Fig. 5.3 and was as follows: light from the source (superluminiscent diode with central wavelength $\lambda = 810$ nm) was led through an optical fiber into collimator (FC), in front of which was a mirror reflecting the outcoming light in right angle into free space. A 50:50 beam splitter divided the beam into two, travelling in perpendicular directions. Mirrors were placed in both arms to send the beams back to the beam splitter, behind which they overlapped again, but this time with an optical path difference. Two more mirrors followed to extend the path of the overlapped beams, as it is important to be sure they do not diverge in longer distance. The last component was a detector (Thorlabs) connected to an oscilloscope. One of the mirrors was placed on a linear stage with micrometric screw for easy adjusting of the optical path, the second mirror was attached to a piezoelectric transducer (PZT). The optical path difference was adjusted carefully by the micrometric screw and scanned by the PZT on the scale of few wavelengths.

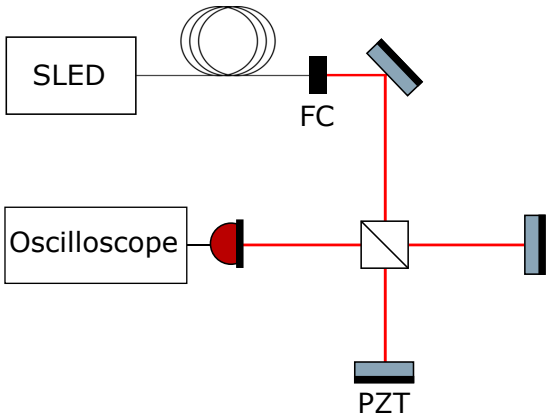

Figure 5.3: A slightly simplified schema of the experimental setup for Fourier-transform spectroscopy based on Michelson's interferometer.

Once the Michelson's interferometer was built and interference was found on the oscilloscope, the measurement of coherence length took place. The interference was seen on the oscilloscope (Rhode and Schwarz) as a sine-like function. By adjusting the micrometric screw and thus shifting the mirror, it was possible to change the optical path difference with which the beams coming from the two arms of the interferometer meet on the detector. As interference depends on this difference greatly, the intensity of the interference was changing correspondingly to the movement of the mirror. This allowed us to measure the coherence length of a particular source.

Interference of the highest intensity (and thus the best visibility) was found by moving the micrometric screw. The visibility was calculated at this point according to (5.1), where the intensity was replaced by the value of voltage

shown on the oscilloscope. Then the screw was being moved to one side till $1/e$ of the value of the highest visibility was experimentally reached. The same was done to the other side from the maximum intensity. The sum of the distance by which the micrometric screw was moved to both sides equals twice the coherence length. From (5.2) we can express $\Delta\lambda$, the width of the source emission spectrum at $1/e$ of the maximum value we are looking for:

$$\Delta\lambda = \sqrt{\frac{2\ln 2}{\pi}}\frac{\lambda^2}{L}. \tag{5.3}$$

The uncertainty $u(\Delta\lambda)$ of the spectral widths at $1/e$ of the maximum value obtained by Fourier-transform spectroscopy was determined using the formula (5.3),

$$u(\Delta\lambda) = \left|\frac{\mathrm{d}(\Delta\lambda)}{\mathrm{d}L}\right| u(L), \tag{5.4}$$

the uncertainty $u(L)$ was set to be 10 µm considering the micrometric screw smallest division. For the superluminescent diode alone, not affected by any filter, the measured coherence length $L = 17$ µm and the calculated spectral width is $\Delta\lambda = (26 \pm 15)$ nm. In the next step, a 3 nm polarization filter was added into the setup. By performing the same measurement as in the previous case, a value $L = 146$ µm was achieved, which corresponds to $\Delta\lambda = (3.0 \pm 0.2)$ nm.

The last spectra measurement involved the Bragg grating (Safibra) and the width of the reflection from the grating was measured. The setup used until now had to be adjusted by adding the circulator as described in Sec. 5.1. The reflection from the grating was brought to the interferometer input. From this point on, the measuring process was the same as in the previous cases. Only the equation (5.1) had to be adjusted as there appeared -28 mV offset on the oscilloscope. In the formula, the value of the offset had to be subtracted twice from the denominator, because by making the sum of U_{max} and U_{min} it was added twice. In the numerator, on the other hand, it was annulled. The offset was only visible and important in the case of FBG, because in the two previous cases there was much more signal reaching the detector and the offset was so small that it would not manifest in the computed spectral widths together with their uncertainties. The measured coherence length of the FBG reflection was $L = 1473$ µm and its calculated spectral width is $\Delta\lambda = (0.296 \pm 0.002)$ nm.

For comparison of the results obtained from Fourier-transform spectroscopy and from the spectrometer with values stated by manufacturers, see Tab. 5.1. Only note that the values specified by the manufacturer represent the FWHM, the experimentally obtained values are the full widths at $1/e$ of the maximum value, they should thus be higher as already mentioned earlier. It is evident that Fourier-transform spectroscopy offers much more accurate results for very narrow spectra. In case of wide spectra, Fourier-transform spectroscopy is however associated with rather a large uncertainty and it is thus more suitable to use the spectrometer.

Source	Spectral width [nm]		
	FT spectroscopy	Spectrometer /± 0.021	Manufacturer
SLED	26 ± 15	29.578	21.32
SLED + 3 nm filter	3.0 ± 0.2	3.456	3
FBG reflection	0.296 ± 0.002	1.090	0.27

Table 5.1: Spectral widths of three different sources obtained from Fourier-transform spectroscopy, from Ocean Optics HR2000+ Spectrometer and values declared by manufacturers.

Chapter 6

Conclusions and outlook

The focus of this thesis was to introduce fiber gratings, devices that play an important role in optical metrology and communications. One can distinguish between short-period (FBG) and long-period (LPFG) fiber gratings. The principle of their operation is based on coupling between modes. The fundamental core mode couples to the same, but opposite travelling core mode in case of FBG, and to several radiant cladding modes in case of LPFG, both groups of fiber gratings can therefore have different usages. In the beginning of this thesis, basic theory connected to fiber gratings is introduced. They operate as diffraction gratings which are induced by a periodical change of refractive index in the fiber core, either by exposure to powerful radiation leading to a permanently inscribed grating, or by mechanical pressure applied periodically on the fiber.

In Chapter 3, fabrication and analysis of the effect of long-period fiber gratings are described. The possibility of mechanically induced periodical refractive index change in the fiber is explored, LPFGs were fabricated by two techniques, 3D printing and milling. They were then pressed against an optical fiber and the source transmission spectrum was observed. Loss notches appeared in the spectrum at certain coupling wavelengths dependent on the grating period. It was confirmed that 3D printed and milled gratings of the same period cause coupling at the same wavelength. Better results, i.e. deeper loss notches even with smaller applied pressure, were achieved at telecommunication wavelengths. The dependence of the coupling wavelength on the period of the grating was determined experimentally as well as predicted numerically. A reasonable correspondence of the experimental data points and the model was achieved, considering the extreme sensitivity of the effective indices computation to the input technical parameters, which were not known as precisely as would have been needed, and it can thus explain the remaining discrepancy. The obtained data points clearly show an existence of the branches respective to different cladding modes and a correct dependence of the coupling wavelength on the grating period.

A significant application area of fiber gratings is sensing. Chapter 4 is hence devoted to experimental measurement of temperature dependence of the coupling wavelength. No explicit and convincing dependence was, however, obtained for LPFGs. The transmission spectra were often damaged after the whole measuring process, which can be attributed to the thermal expansion of the Peltier element used to set the required temperature and also to the influence

on the fiber buffer, which was removed for further measurements and it resulted in a better stability of the transmission spectra. Our LPFGs are therefore unsuitable to be used in temperature sensing. However, no significant temperature dependence of the coupling wavelength may be useful for other applications that require temperature stability, for example sensing of the refractive index of the surroundings. The temperature dependence was also measured for a commercially acquired fiber Bragg grating with central wavelength $\lambda_B = 809.97$ nm and as a result, the average temperature sensitivity was determined to be 7.6 pm/K, which will be later useful when different kinds of measurements are performed with this particular FBG.

Finally, the last chapter deals with methods of optical spectra measurement, namely grating spectrometers and Fourier-transform spectroscopy. Spectra of different widths were examined by both methods. The result is that for wider spectra, it is more convenient and accurate to use the grating spectrometer, for a very narrow spectra, on the other hand, it is necessary to choose a different method as the resolution limit of the spectrometer is reached, and Fourier-transform spectroscopy offers very accurate results in such cases.

Nowadays 3D printers are widely expanding, becoming more attainable and the achievable resolution is improving. This will make it possible to further improve the fabrication of long-period fiber gratings and increase their availability. The precisely fabricated mechanically induced LPFGs can then be used for generating frequency-flat pulses or for various sensing applications, their huge advantage being the fact that their effect upon an optical fiber is only temporary and thus enables repeated usage of the fiber, either with different gratings or even for completely different purposes.

Bibliography

[1] K. O. Hill, Y. Fujii, D. C. Johnson, and B. S. Kawasaki, "Photosensitivity in optical fiber waveguides: Application to reflection filter fabrication," *Applied Physics Letters*, vol. 32, no. 10, pp. 647–649, 1978.

[2] A. Othonos, "Fiber Bragg gratings," *Review of Scientific Instruments*, vol. 68, no. 12, pp. 4309–4341, 1997.

[3] T. Erdogan, "Fiber grating spectra," *Journal of Lightwave Technology*, vol. 15, no. 8, pp. 1277–1294, 1997.

[4] Y. Rao, T. Zhu, Z. Ran, Y. Wang, J. Jiang, and A. Hu, "Novel long-period fiber gratings written by high-frequency CO_2 laser pulses and applications in optical fiber communication," *Optics Communications*, vol. 229, no. 1-6, pp. 209–221, 2003.

[5] Y. Wang, "Review of long period fiber gratings written by CO_2 laser," *Journal of Applied Physics*, vol. 108, no. 8, p. 081101, 2010.

[6] S. Savin, M. J. F. Digonnet, G. S. Kino, and H. J. Shaw, "Tunable mechanically induced long-period fiber gratings," *Optics Letters*, vol. 25, no. 10, p. 710, 2000.

[7] A. M. Vengsarkar, N. S. Bergano, C. R. Davidson, J. R. Pedrazzani, J. B. Judkins, and P. J. Lemaire, "Long-period fiber-grating-based gain equalizers," *Optics Letters*, vol. 21, no. 5, p. 336, 1996.

[8] K. Hill, B. Malo, K. Vineberg, F. Bilodeau, D. Johnson, and I. Skinner, "Efficient mode conversion in telecommunication fibre using externally written gratings," *Electronics Letters*, vol. 26, no. 16, p. 1270, 1990.

[9] F. Bilodeau, K. Hill, B. Malo, D. Johnson, and I. Skinner, "Efficient, narrowband $LP_{01} \leftrightarrow LP_{02}$ mode convertors fabricated in photosensitive fibre: spectral response," *Electronics Letters*, vol. 27, no. 8, p. 682, 1991.

[10] A. Vengsarkar, P. Lemaire, J. Judkins, V. Bhatia, T. Erdogan, and J. Sipe, "Long-period fiber gratings as band-rejection filters," *Journal of Lightwave Technology*, vol. 14, no. 1, pp. 58–65, 1996.

[11] X. Gu, W. Mohammed, L. Qian, and P. W. E. Smith, "All-fiber laser beam shaping using a long-period grating," *IEEE Photonics Technology Letters*, vol. 20, no. 13, pp. 1130–1132, 2008.

[12] W. Mohammed and X. Gu, "Long-period grating and its application in laser beam shaping in the 10 µm wavelength region," *Applied Optics*, vol. 48, no. 12, p. 2249, 2009.

[13] V. Bhatia and A. M. Vengsarkar, "Optical fiber long-period grating sensors," *Optics Letters*, vol. 21, no. 9, p. 692, 1996.

[14] V. Bhatia, T. D'Alberto, K. A. Murphy, R. O. Claus, and A. M. Vensarkar, "Optical fiber long-period grating sensors," in *Optical Fiber Sensors*, OSA, 1996.

[15] S. W. James and R. P. Tatam, "Optical fibre long-period grating sensors: characteristics and application," *Measurement Science and Technology*, vol. 14, no. 5, pp. R49–R61, 2003.

[16] H. Patrick, A. Kersey, and F. Bucholtz, "Analysis of the response of long period fiber gratings to external index of refraction," *Journal of Lightwave Technology*, vol. 16, no. 9, pp. 1606–1612, 1998.

[17] J. H. Chong, P. Shum, H. Haryono, A. Yohana, M. Rao, C. Lu, and Y. Zhu, "Measurements of refractive index sensitivity using long-period grating refractometer," *Optics Communications*, vol. 229, no. 1-6, pp. 65–69, 2004.

[18] G. Quero, M. Consales, R. Severino, P. Vaiano, A. Boniello, A. Sandomenico, M. Ruvo, A. Borriello, L. Diodato, S. Zuppolini, M. Giordano, I. C. Nettore, A. Colao, P. E. Macchia, F. Santorelli, A. Cutolo, and A. Cusano, "High sensitive long period fiber grating biosensor for cancer biomarker detection," in *Proceedings of the 9th International Joint Conference on Biomedical Engineering Systems and Technologies*, SCITEPRESS - Science and and Technology Publications, 2016.

[19] Y. Zhao, S. Liu, J. Luo, Y. Chen, C. Fu, C. Xiong, Y. Wang, S. Jing, Z. Bai, C. Liao, and Y. Wang, "Torsion, refractive index, and temperature sensors based on an improved helical long period fiber grating," *Journal of Lightwave Technology*, vol. 38, no. 8, pp. 2504–2510, 2019.

[20] B. E. A. Saleh and M. C. Teich, *Fundamentals of photonics; 2nd ed.* Wiley series in pure and applied optics, New York, NY: Wiley, 2007.

[21] B. Tahir, J. Ali, and R. Rahman, "Fabrication of fiber grating by phase mask and its sensing application," *Journal of Optoelectronics and Advanced Materials*, vol. 8, pp. 1604–1609, 2006.

[22] T. Erdogan, "Cladding-mode resonances in short- and long-period fiber grating filters," *Journal of the Optical Society of America A*, vol. 14, no. 8, p. 1760, 1997.

[23] T. Erdogan, "Cladding-mode resonances in short- and long-period fiber grating filters: errata," *Journal of the Optical Society of America A*, vol. 17, no. 11, p. 2113, 2000.

[24] M. N. Ng, Z. Chen, and K. S. Chiang, "Temperature compensation of long-period fiber grating for refractive-index sensing with bending effect," *IEEE Photonics Technology Letters*, vol. 14, no. 3, pp. 361–362, 2002.

[25] K. Shima, K. Himeno, T. Sakai, S. Okude, A. Wada, and R. Yamauchi, "A novel temperature-insensitive long-period fiber grating using a boron-codoped-germanosilicate-core fiber," in *Proceedings of Optical Fiber Communication Conference (OFC'97)*, 1997.

[26] J.-N. Jang, S. Y. Kim, S.-W. Kim, and M.-S. Kim, "Temperature insensitive long-period fibre gratings," *Electronics Letters*, vol. 35, no. 24, p. 2134, 1999.

[27] M. Born, E. Wolf, A. B. Bhatia, P. C. Clemmow, D. Gabor, A. R. Stokes, A. M. Taylor, P. A. Wayman, and W. L. Wilcock, *Principles of Optics*. Cambridge University Press, 1999.

[28] C. Akcay, P. Parrein, and J. P. Rolland, "Estimation of longitudinal resolution in optical coherence imaging," *Applied Optics*, vol. 41, no. 25, p. 5256, 2002.